Calculating the Eroded Thickness Corresponding to a Short-Term Tectonic Uplift with Milankovitch Theory: A Case Study of the Middle Permian Maokou Formation in Southeastern Sichuan Basin, Southwest China

Siyu Shi, Wenlong Ding,* Gang Zhao, Zikang Xiao, Yuntao Li, and Baocheng Jiao

Read Online

ACCESS | Metrics & More | Article Recommendations

Calculating eroded thickness corresponding to a short-term tectonic uplift with Milankovitch theory
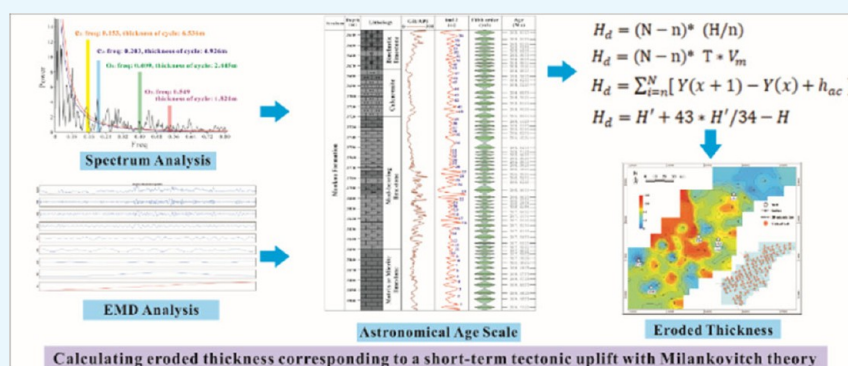
ABSTRACT: The Middle Permian Maokou Formation in the southeastern Sichuan Basin is a typical carbonate karst reservoir. At the end of the Middle Permian, a short-term tectonic uplift (Tungwu movement) occurred in the upper Yangtze region, causing the formation of dissolved fissures and holes. To determine the location of the high-quality reservoir, this paper calculated the eroded thickness using the Milankovitch theory. Based on the gamma logging data of the six wells in the southeastern Sichuan Basin, the dominant frequency and the astronomical time scale were evaluated via frequency spectrum analysis, continuous wavelet transform, and empirical mode decomposition. In addition, we analyzed the relationship between Fischer curve characteristics and the variation of lithology. Last, four methods were used to calculate the eroded thickness, and the rationality was analyzed. Consequently, we identified four levels of Milankovitch cycles, i.e., middle eccentricity (e_2), short eccentricity (e_3), long obliquity (o_1), and short obliquity (o_2). Also, the Fischer curves of the six wells were divided into two forms related to local structural uplift. The residual strata of the Maokou Formation comprised three complete third-order cycles, and the boundaries were the 15th, 34th, and 54th e_3 cycles. The deposition rate of bioclastic limestone was the lowest (2.12–5.36 cm/ka with an average of 3.30 cm/ka), whereas the deposition rate of argillaceous limestone was the largest (2.27–5.25 cm/ka with an average of 4.09 cm/ka). Among the four methods, the missing formation deposition rate method exhibited the most precise calculation results, while that of the seismic data method was relatively low. Generally, the eroded thickness of the Maokou Formation in southeastern Sichuan was in the range of 0–140 m, i.e., the eroded thickness in the west and south of X14 was relatively large (>100 m), while the area north of LS1 experienced the weakest denudation (eroded thickness < 40 m).

1. INTRODUCTION

Denudation can be defined as a geological phenomenon in which the moving medium destroys the surface rocks and causes the products to peel off the original place. Strong denudation can lead to the missing surface strata (formation of unconformity) and changes in reservoir pore structure. In general, denudation can create more space for oil and gas seepage and storage.[1−3] Eroded thickness calculation is vital for a broad range of scientific and oil/gas industrial processes. It plays a pivotal role in analyzing the concept of burial history, structural evolution, paleogeomorphology, hydrocarbon generation, oil/gas preser-

vation condition, and the distribution of carbonate karst. Researchers initially analyzed the intensity of denudation based on the residual formation thickness rather than directly
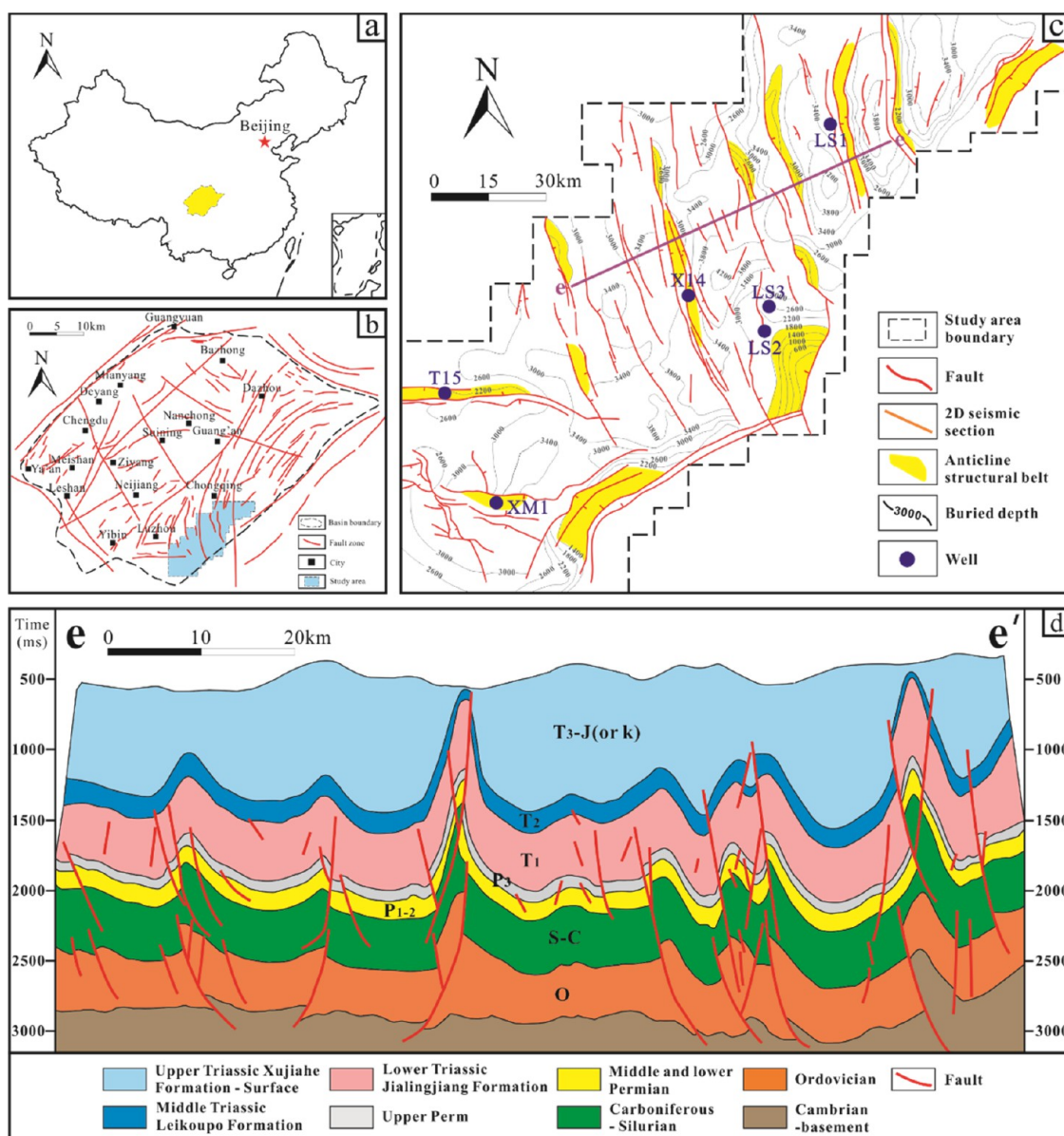
Figure 1. (a) Location of Sichuan province; (b) distribution of faults in the Sichuan Basin and the location of the study area; (c) distribution of faults, burial depth of the top surface of the Maokou Formation in the study area, and the location of six wells; (d) e−e′ 2D seismic interpretation profile.

calculating the eroded thickness. In 1976, Magara[4] discovered a discontinuity of the mud shale compaction curve at the unconformity and proposed a method to calculate the eroded thickness using acoustic logging data (acoustic time difference method). Based on the positive correlation between vitrinite reflectance (Ro) and the burial depth of the source rock, Dow[5] proposed a vitrinite reflectance method to calculate the eroded thickness (Ro method) in 1977. Elsewhere, in 1978, Van Hinte[6] found a correspondence between the deposition rate and the absolute geological age and then put forward a deposition rate method, while Guidish et al.[7] improved the method in 1985. In 1987, Laslett et al.[8] established a cooling process during the denudation based on the various characteristics of five indicators of apatite fission track and proposed the apatite fission track method. Additionally, in 1996, Li and Li[9] believed that the low average concentration of natural gas in the discontinuous formation was associated with the lack of formation. In addition, they proposed a method for calculating the eroded thickness using the equilibrium concentration of natural gas. Since the

1990s, due to the widespread application of the Milankovitch Earth Orbital Period Theory in the field of sedimentary stratigraphy,[10−13] numerous scholars began to apply the Milankovitch theory in the calculation of the eroded thickness.[14−16] In addition, the cosmogenic nuclide method has been applied in a number of regions.[17]

Notably, the Dongwu movement, a crustal uplift caused by the upwelling of the Emei Mountain mantle plume, occurred at the end of the Middle Permian (about 260 Ma ago). The Dongwu movement caused the formation of ancient uplift centered on the present-day Luzhou City and the denudation of the Maokou Formation. Several lines of evidence suggest that the dissolution pores of the Maokou Formation are related to surface leaching, organic matter evolution, diagenesis, and hydrothermal fluids, but the surface leaching caused by denudation is the main factor in the change of the pore structure of the reservoir.[18−22]

The development of numerous karst reservoirs is usually based on long-term tectonic uplift and strong denudation.[23−27] In contrast, the Dongwu movement was a short-term tectonic
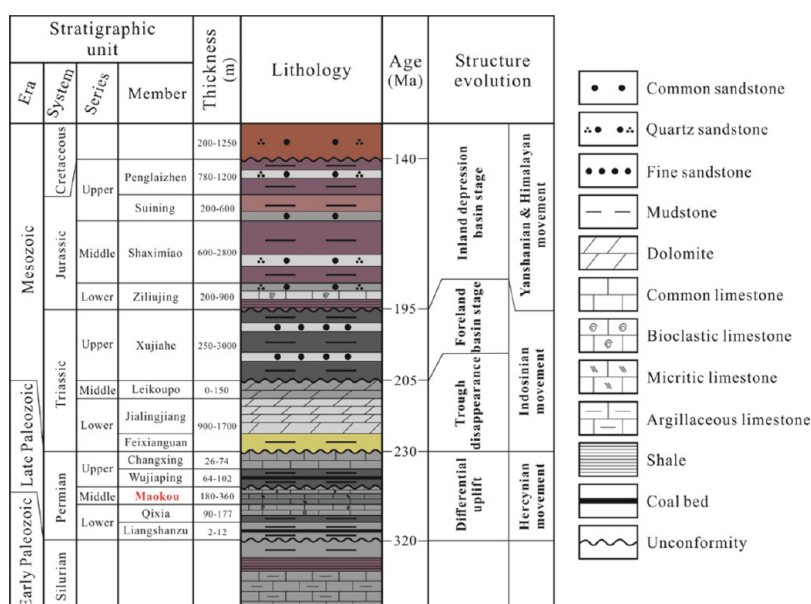
Figure 2. Stratigraphic characteristics of the study area.

uplift, with a duration of about 0.5−2.5 Ma.[28] Several studies revealed that the residual thickness of the Maokou Formation in the Sichuan Basin varies from 180 to 360 m,[29] and the maximum eroded thickness does not exceed 200 m.[30] In addition, the residual thickness is greater than the eroded thickness. Therefore, it is vital to eliminate the influence of the original thickness difference on the calculation results when calculating the eroded thickness. The formation thickness comparison and impression methods ignore the difference in the original thickness of the formation, and the resulting calculation error is unacceptable. Additionally, the maximum eroded thickness is less than 200 m, and the "vitrescence reflectance-buried depth" curve cannot show apparent discontinuities at the unconformity; hence, the vitrinite reflectance method was unsuitable for this study. The Maokou Formation is dominated by carbonate rocks and a few thick pure mudstones; thus, the acoustic time difference method cannot be used. Furthermore, due to the limitations on sample size and the requirements of calculation accuracy, the apatite fission-track method, natural gas equilibrium concentration method, and cosmogenic nuclide method were unsuitable for this work.

To exclude the influence of the original thickness difference on the calculation results, it is essential to calculate the original thickness. During a continuous deposition process, the astronomical cycles experienced by each region in a similar deposition system were consistent and can be recorded by formation. Nevertheless, different regions have different deposition rates at the same time. Therefore, if the missing number of astronomical cycles and average deposition rate of the eroded formation can be estimated, then the original and eroded thicknesses can be calculated. To analyze the eroded thickness distribution of the Maokou Formation, the periods of seven astronomical cycles of the Middle Permian were calculated. The dominant frequency signal contained in the residual strata was identified based on spectrum analysis and wavelet transform methods. Using the empirical mode decomposition (EMD) method, we established astronomical age scales of the six wells. Moreover, we evaluated the relationship between the Fischer curve and the lithology combination and identified a system tract. The deposition rates of different lithologies in the six wells

were calculated. Finally, four methods were used to calculate the eroded thickness of the Maokou Formation in southeastern Sichuan, and the distribution was analyzed. Our findings provide fundamental insights into the calculation of eroded thickness during a short-term tectonic uplift and provide a valuable basis for future studies.

2. GEOLOGICAL SETTING

The study area was the southeast of Sichuan Basin, an area dominated by NNW−SSE syncline anticline structural belts, and a relatively small number of N−W and NE−SW syncline structural belts. The burial depth of the top surface of the Maokou Formation was 2500−4000 m, and the variation of the burial depth was mainly related to the anticline structure (Figure 1). Vertically, controlled by the mud shale slip layer at the bottom of the Silurian and the gypsum slip layer at the top of the Cambrian, the double-slippage faults were well developed.[31]

Being influenced by the Hercynian Movement, Indosinian Movement, Yanshan Movement, and Himalayan Movement, Devonian, Carboniferous, and Cenozoic strata were extensively missing in the study area, and six vital unconformities were developed (Figure 2). Since the Eopaleozoic era, the study area has gone through four stages, i.e., differential uplift-trough disappearance−foreland basin−inland depositional basin. Correspondingly, the lithology gradually changed from carbonate rocks of Permian and Early Triassic to clastic rocks. Notably, tight limestone is the dominant rock type of the Maokou Formation in southeastern Sichuan, including common limestone (matrix limestone or micrite limestone), mud-bearing limestone, argillaceous limestone, calcarenite, and bioclastic limestone.

3. RESULTS AND DISCUSSION

3.1. The Astronomical Cycle Period in the Middle Permian. The stars of the solar system produce a superimposed gravitational field on the Earth, which periodically changes and causes periodic variation in orbital parameters of the Earth. The theory of Milankovitch confirms that the periodic variation in orbital parameters of the Earth is the direct trigger of climate

change and indirectly regulates the sedimentary process.[32,33] There exist three types of Milankovitch orbital cycles, including eccentricity, obliquity, and precession. The eccentricity is the degree to which the orbit deviates from a perfect circle, where the change frequency is lower, while the period is longer. Obliquity is the angle between the orbital surface and equatorial surface of the Earth whose changing frequency is higher compared to the eccentricity, while the period is relatively short. The long-term shifting in the rotation axis of the Earth caused the vernal equinox to move westward along the ecliptic, resulting in a phenomenon called precession, where the solar year is shorter compared to the sidereal year. It has the highest changing frequency and the shortest period.

Eccentricity period is relatively stable with a long eccentricity period (e_1) of 405 kyr, a medium eccentricity period (e_2) of 125 kyr, and a short eccentricity period (e_3) of 95 kyr. In contrast, the cycle of obliquity and precession changes with the geologic period. In 1992, Berger et al. calculated the long obliquity period (o_1), short obliquity period (o_2), long precession period (σ_1), and short precession period (σ_2) of 11-time nodes,[34] and the four astronomical orbit periods showed an apparent negative correlation with the geological age (Figure 3). The deposition
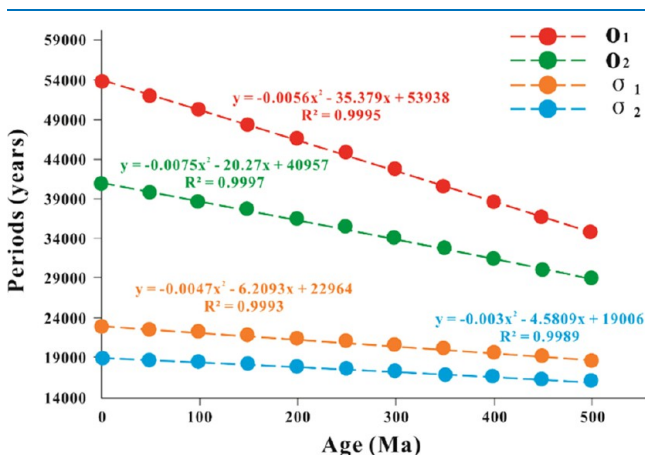
Figure 3. Period variation of obliquity and precession. (The original data come from Berger et al.[34])

period of the Middle Permian Maokou Formation was 268.8 to 259.8 Ma.[28] A median of 264.3 Ma was considered as the time node of the Maokou Formation sedimentation; in addition, o_1, o_2, σ_1, and σ_2 were calculated using the above linear equation, which were 44.20 ka, 35.08 kyr, 20.99 kyr, and 17.59 kyr, respectively.

3.2. Identification of the Milankovitch Cycle.
3.2.1. Dominant Frequency Analysis of GR Logging Data. In cycle analysis, extracting the dominant frequency of sedimentary cycles from electrical signals is vital. Notably, spectrum analysis based on GR logging data is presently a relatively mature method. The time-domain signal can be converted into a frequency-domain signal by Fourier transform. The curve with similar frequency-domain signal intensity to the vertical axis and the frequency to the horizontal axis was the spectrum curve. In the spectrum curve, the dominant frequency is the frequency with higher signal strength. The value of the dominant frequency was negatively correlated with the corresponding cycle period.

PAST software was used to perform spectrum analysis based on the GR logging data of the six wells,[35] and we extracted the

frequency with a confidence level greater than 95% as the dominant frequency (Figure 4). The dominant frequency of the six wells is shown in Table 1.

3.2.2. Extraction of Dominant Frequency Containing Milankovitch Cycle Information. The Milankovitch cycle can be recorded by sedimentary formation; however, not all dominant frequency information is related to it. To extract the dominant frequency with Milankovitch cycle information, a certain connection needs to be established between them. If the ratios of the frequencies in several sedimentary cycles are close to that of several Milankovitch cycles, then the formation is considered to be influenced by the Milankovitch cycles.

We calculated the frequency ratios of the seven astronomical cycles of the Middle Permian (Table 2). The f in Table 2 represents the alternating frequency of Milankovitch's astronomical cycles (such as various types of eccentricity, obliquity, and precession). It is the reciprocal of time (period), which can be understood as alternating once every certain time. We compared the frequency ratios with the ratios of the dominant frequency of each well. The ratios of the dominant frequencies close to that of the astronomical cycle frequencies (e_2, e_3, o_1, and o_2) were found in four wells (LS1, LS2, LS3, and X14), while the ratios of the dominant frequencies close to that of the frequencies (e_2, e_3, and o_1) were found in two wells (T15 and XM1) (Table 3). The error was within the range of 0.13 to 6.01%, with an acceptable average error of 2.38%, indicating that the Milankovitch cycle was recorded during the sedimentary process of the Maokou Formation, which was consistent with the research result of Cong et al.[36]

The dominant frequency had the following relationship with sediment thickness

$$h_c = \frac{1}{f} \tag{1}$$

where h_c represents the sediment thickness (m), and f represents the dominant frequency, which can be understood as alternating every time a certain thickness is deposited. Based on this formula, we calculated the sediment thickness of the four cycles, i.e., e_2, e_3, o_1, and o_2 of each well (Table 3 and Figure 4).

3.2.3. The Rationality of Milankovitch Cycle Identification Results. Continuous wavelet transform extracts information of different scales contained in the logging signal and converts it into time domain and frequency domain information, which helps in revealing the hidden cyclicity in the formation.[37] As shown in Figure 5, the frequency band corresponding to the Milankovitch cycle in each well covered more high-energy signals, indicating that the dominant frequencies corresponding to the Milankovitch cycle were representative.

To evaluate the rationality of the Milankovitch cycle identification results for each well, it is also necessary to verify the consistency of the deposition rate corresponding to the cycle with the overall deposition rate variation range of the Middle Permian Maokou Formation in the Sichuan Basin. Based on the analysis of stratigraphic characteristics, sedimentary characteristics, and lithofacies paleogeography, He et al.[28] explored the geodynamic background and evolution of the Dongwu movement and calculated the maximum denudation duration using the denudation rate of carbonate rocks in the humid tropical zone for the Upper Yangtze area, which varied from 0.5 to 2.5 Ma. As mentioned above, the thickness of the Middle Permian Maokou Formation in southeastern Sichuan varied from 180 to 360 m. Therefore, it can be estimated that the deposition duration of the Middle Permian Maokou Formation in southern
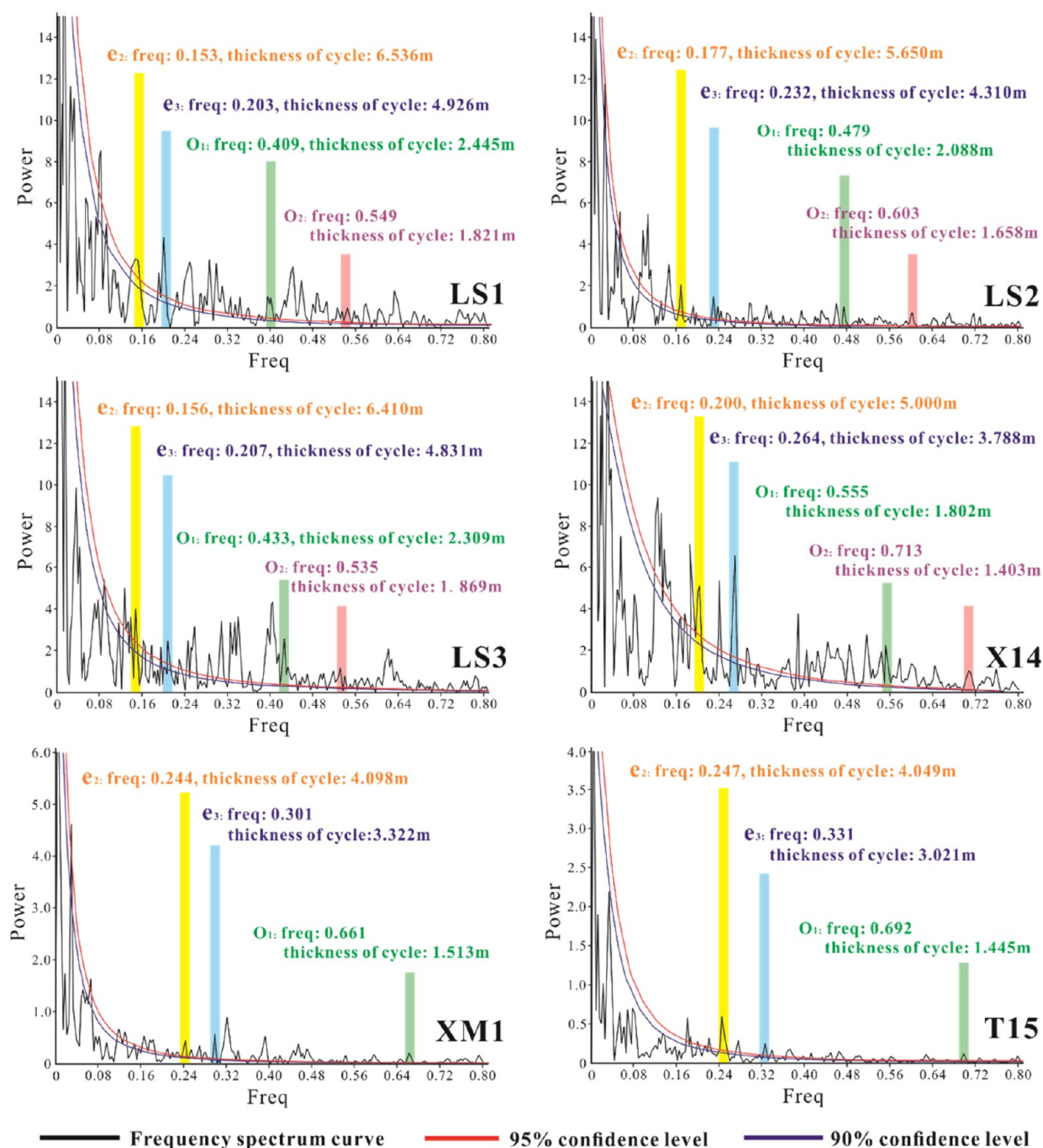
Figure 4. Spectrum analysis diagram of GR logging data of the Maokou Formation in the study area.

Sichuan was about 6.5 to 8.5 Ma, while the average deposition rate varied from 2.12 to 5.54 cm/ka.

Table 4 shows the average deposition rates corresponding to each Milankovitch cycle of the six wells. The calculation results were in the range of the average deposition rate, indicating that the identification results of the Milankovitch cycle were reasonable and represent the response of the astronomical orbital period to the sedimentary event.

3.3. Establishment of an Astronomical Age Scale Based on the Empirical Mode Decomposition (EMD) Method. Establishing an astronomical time scale involves establishing a relationship between stratum depth, sedimentary cycle, and geological age. The first step in this process involves extracting cyclic waves based on logging data. Filtering is one of

the most widely used methods in identifying sedimentary cycles, specifically wavelet filtering and Gaussian filtering.[14] Because of the difference in calculation methods, it is essential to select a suitable wavelet based on the analysis of astronomical cycles. In recent years, increasing research used the empirical formula decomposition (EMD) method to study the sedimentary cycle.[33,38,39] This method extracts several relatively simple and stable components imf of different frequencies from a complex signal. Also, the signal decomposition is based on the characteristics of the data itself, and no basis function is set in advance. In contrast, the EMD method is more convenient and retains additional and vital geological information, which is more suitable for the study of carbonate sedimentary cycles.

Table 1. Dominant Frequency of GR Logging Data in the Maokou Formation of Six Wells

well	dominant frequency of GR logging data
LS1	0.097, 0.153, 0.203, 0.212, 0.259, 0.296, 0.309, 0.352, 0.409, 0.465, 0.496, 0.543, 0.636, 0.549, 0.754, 0.770, 0.786, 0.798, 0.832, 0.8454, 0.867, 0.910, 0.988, 1.020
LS2	0.054, 0.102, 0.110, 0.177, 0.212, 0.232, 0.241, 0.263, 0.303, 0.331, 0.397, 0.436, 0.479, 0.510, 0.535, 0.541, 0.603, 0.646, 0.671, 0.717, 0.728, 0.841
LS3	0.105, 0.141, 0.156, 0.176, 0.190, 0.207, 0.226, 0.240, 0.256, 0.267, 0.295, 0.317, 0.334, 0.342, 0.347, 0.402, 0.411, 0.433, 0.474, 0.504, 0.524, 0.535, 0.623, 0.640, 0.684, 0.706, 0.736, 0.761
X14	0.109, 0.152, 0.158, 0.164, 0.194, 0.200, 0.215, 0.228, 0.264, 0.291, 0.316, 0.388, 0.422, 0.400, 0.458, 0.476, 0.498, 0.555, 0.589, 0.613, 0.653, 0.713, 0.750, 0.765, 0.868, 0.977, 1.026
T15	0.182, 0.188, 0.202, 0.223, 0.247, 0.277, 0.329, 0.331, 0.373, 0.397, 0.411, 0.449, 0.462, 0.503, 0.545, 0.562, 0.623, 0.692, 0.723, 0.750, 0.781, 0.795
XM1	0.070, 0.124, 0.134, 0.170, 0.180, 0.187, 0.214, 0.244, 0.257, 0.274, 0.301, 0.324, 0.344, 0.371, 0.394, 0.421, 0.447, 0.457, 0.471, 0.544, 0.581, 0.598, 0.648, 0.661, 0.738, 0.761, 0.871

We calculated the seven components (imf.1−imf.7) of the Maokou Formation of the six wells in southeastern Sichuan based on GR logging data (Figure 6), and the number of cycles included in each component was counted. At the same time, the number of each cycle included in the Maokou Formation of each well was calculated based on the thickness of the Maokou Formation and the average thickness of each cycle. An inspection of the data in Table 5 reveals that the number of e_3 cycles in the six wells matches well with the number of cycles included in the component imf.3. Thus, the imf.3 component can be used as the basis for establishing the astronomical time scale. Notably, for the component imf.3, the part between the two troughs was considered as a complete cycle. Nevertheless, incomplete cycles might appear at the top and bottom of the stratum. When counting the number of cycles, incomplete cycles were ignored. Therefore, it was acceptable to have an error less than 2 between the number of e_3 cycles and the cycle number of imf.3.

The number of cycles of the Maokou Formation in LS1 was the smallest, i.e., 49 e_3 cycles, suggesting that LS1 retains the strata deposited within 4.7 Myr. The Maokou Formation of T15 had the largest number of cycles, i.e., 74 e_3 cycles, and the strata deposited within 7.0 Myr were retained. The calculation results were consistent with the conclusion that the Middle Permian Maokou Formation had a maximum deposition duration of 8.5 Ma. The astronomical time scale of the six wells was established (with the period of e_3 cycle as the minimum time scale), and the data of sediment thickness and deposition rate were calculated (Figure 7).

3.4. Characteristic Analysis of the Fischer Plots. In recent years, the Fisher plot has been applied by researchers to analyze the variation of deposition rate and sea-level fluctuations of clastic rocks and carbonate rocks.[40] It regarded the cumulative cycle number as the abscissa and the cumulated migration of average cycle thickness as the ordinate. The cumulative departure from mean cycle thickness was calculated using the following formula

$$H_n = \sum_{i=1}^{n} (h_n - h_{ac}) \tag{2}$$

where H_n represents the cumulated migration of average cycle thickness (m), n represents the number of e_3 cycles in the residual strata, h_n represents the formation thickness of the nth cycle (m), and h_{ac} represents the average cycle thickness (m).

Based on the astronomical time scale of the Maokou Formation, we calculated the thickness of each e_3 cycle and drew the Fischer plots (Figure 8).

In the 1st to 54th cycles, the six wells experienced three third-order cycles where the accommodating space first increased and then decreased, i.e., SQ1, SQ2, and SQ3. Each third-order cycle comprises 15−20 e_3 cycles with a duration of 1.43−1.90 Ma. The sequence boundaries of the three third-order cycles were the strata corresponding to the 15th, 34th, and 54th e_3 cycles, respectively.

The Fischer plots of the six wells were divided into two types. The Fischer curves of LS1, LS2, T15, and XM1 were similar to the reverse V shape (Figure 8a), while the curves of LS3 and X14 were similar to the V shape (Figure 8b). During the 15th to 34th cycles of the reverse V-shaped curve, the accommodating space increased steadily and then decreased slightly. In contrast, the accommodating space of the V-shaped curve increased slightly and then decreased significantly for a long time. The change in accommodating space was influenced by the sea level and basement activity. During the 15th to 34th cycles, the accommodating space increased and then decreased, indicating that the sea level experienced a rising and falling process. The areas of LS3 and X14 might have experienced local basement uplift during this period, causing a reduction in the overall accommodating space. Therefore, the difference in curve shape might be related to local tectonic movement. Regarding lithological characteristics, the curves of the two forms were different. Starting from the 34th cycle, the wells corresponding to the reverse V-shaped curve began to develop common limestone or bioclastic limestone, while the wells corresponding to the V-shaped curve began to develop calcarenite. This was also related to the reduction of the accommodating space and terrigenous minerals.

3.5. Calculation of the Eroded Thickness. *3.5.1. Calculating the Eroded Thickness Based on the Average Cycle Thickness.* Jiang et al. evaluated the distribution of the Maokou Formation in the Sichuan Basin and the influence of the Dongwu movement on paleomorphology. They believed that the area between Chongqing and Fuling experienced weak tectonic uplift during the Dongwu movement, the denudation intensity experienced by the Maokou Formation was low, or the

Table 2. Frequency Ratio of Milankovitch Astronomical Cycles of the Middle Permian

Milankovitch cycle	cycle period (ka)	f	f/fe_1	f/fe_2	f/fe_3	f/fo_1	f/fo_2	$f/f\sigma_1$	$f/f\sigma_2$
e_1	405.00	0.0025	1.000						
e_2	125.00	0.0080	3.240	1.000					
e_3	95.00	0.0105	4.253	1.313	1.000				
o_1	44.20	0.0226	9.157	2.826	2.153	1.000			
o_2	35.08	0.0285	11.535	3.560	2.713	1.260	1.000		
σ_1	20.99	0.0476	19.286	5.952	4.535	2.106	1.672	1.000	
σ_2	17.59	0.0569	23.024	7.106	5.414	2.514	1.996	1.194	1.000

Table 3. Ratio of Dominant Frequency Corresponding to Milankovitch Cycles

well	Milankovitch cycle	dominant frequency	dominant frequency ratio (f/fe_2)	astronomical cycle frequency ratio (f/fe_2)	error	sediment thickness during the cycle (m)
LS1	e_2	0.153	1.000	1.000		6.536
	e_3	0.203	1.327	1.313	1.05%	4.926
	o_1	0.409	2.673	2.826	5.41%	2.445
	o_2	0.549	3.588	3.560	0.79%	1.821
LS2	e_2	0.177	1.000	1.000		5.650
	e_3	0.232	1.311	1.313	0.13%	4.310
	o_1	0.479	2.706	2.826	4.24%	2.088
	o_2	0.603	3.407	3.560	4.31%	1.658
LS3	e_2	0.156	1.000	1.000		6.410
	e_3	0.207	1.327	1.313	1.10%	4.831
	o_1	0.433	2.776	2.826	1.79%	2.309
	o_2	0.535	3.429	3.560	3.67%	1.869
X14	e_2	0.200	1.000	1.000		5.000
	e_3	0.264	1.320	1.313	0.57%	3.788
	o_1	0.555	2.775	2.826	1.81%	1.802
	o_2	0.713	3.565	3.560	0.13%	1.403
T15	e_2	0.247	1.000	1.000		4.049
	e_3	0.331	1.340	1.313	2.10%	3.021
	o_1	0.692	2.802	2.826	0.87%	1.445
XM1	e_2	0.244	1.000	1.000		4.098
	e_3	0.301	1.234	1.313	6.01%	3.322
	o_1	0.611	2.709	2.826	4.14%	1.513
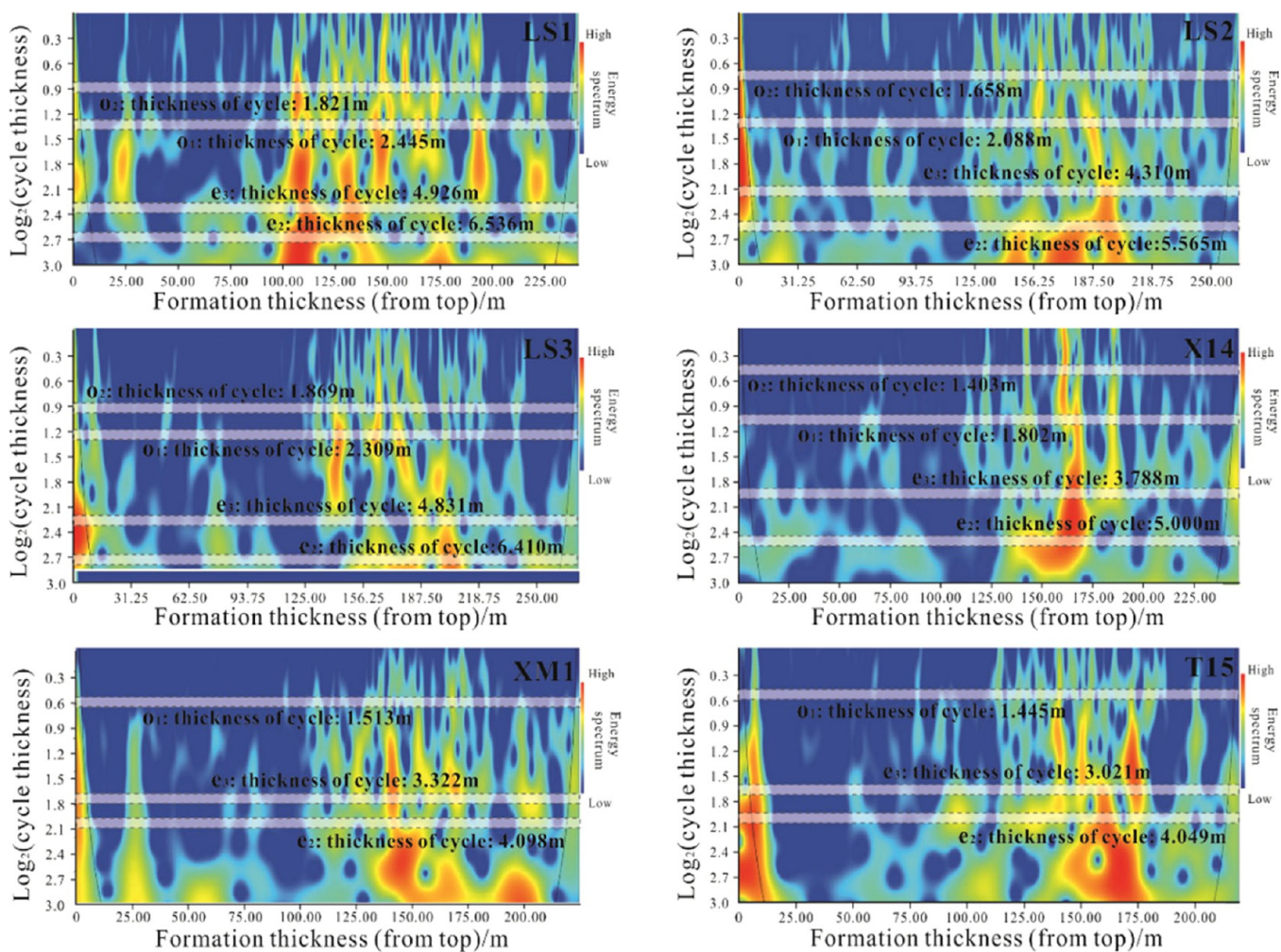
Figure 5. Wavelet transform analysis diagram of GR logging data of the Maokou Formation in the study area.

Table 4. Deposition Rate of Dominant Frequency Corresponding to Milankovitch Cycles

well	e_2 cycle thickness (m)	average deposition rate of e_2 cycle (cm/ka)	e_3 cycle thickness (m)	average deposition rate of e_3 cycle (cm/ka)	o_1 cycle thickness (m)	average deposition rate of o_1 cycle (cm/ka)	o_2 cycle thickness (m)	average deposition rate of o_2 cycle (cm/ka)
LS1	6.536	5.23	4.926	5.19	2.445	5.53	1.821	5.20
LS2	5.650	4.52	4.310	4.54	2.088	4.73	1.658	4.73
LS3	6.410	5.13	4.831	5.09	2.309	5.23	1.869	5.33
X14	5.000	4.00	3.788	3.99	1.802	4.08	1.403	4.00
T15	4.049	3.24	3.021	3.18	1.445	3.27		
XM1	4.098	3.28	3.322	3.50	1.513	3.43		
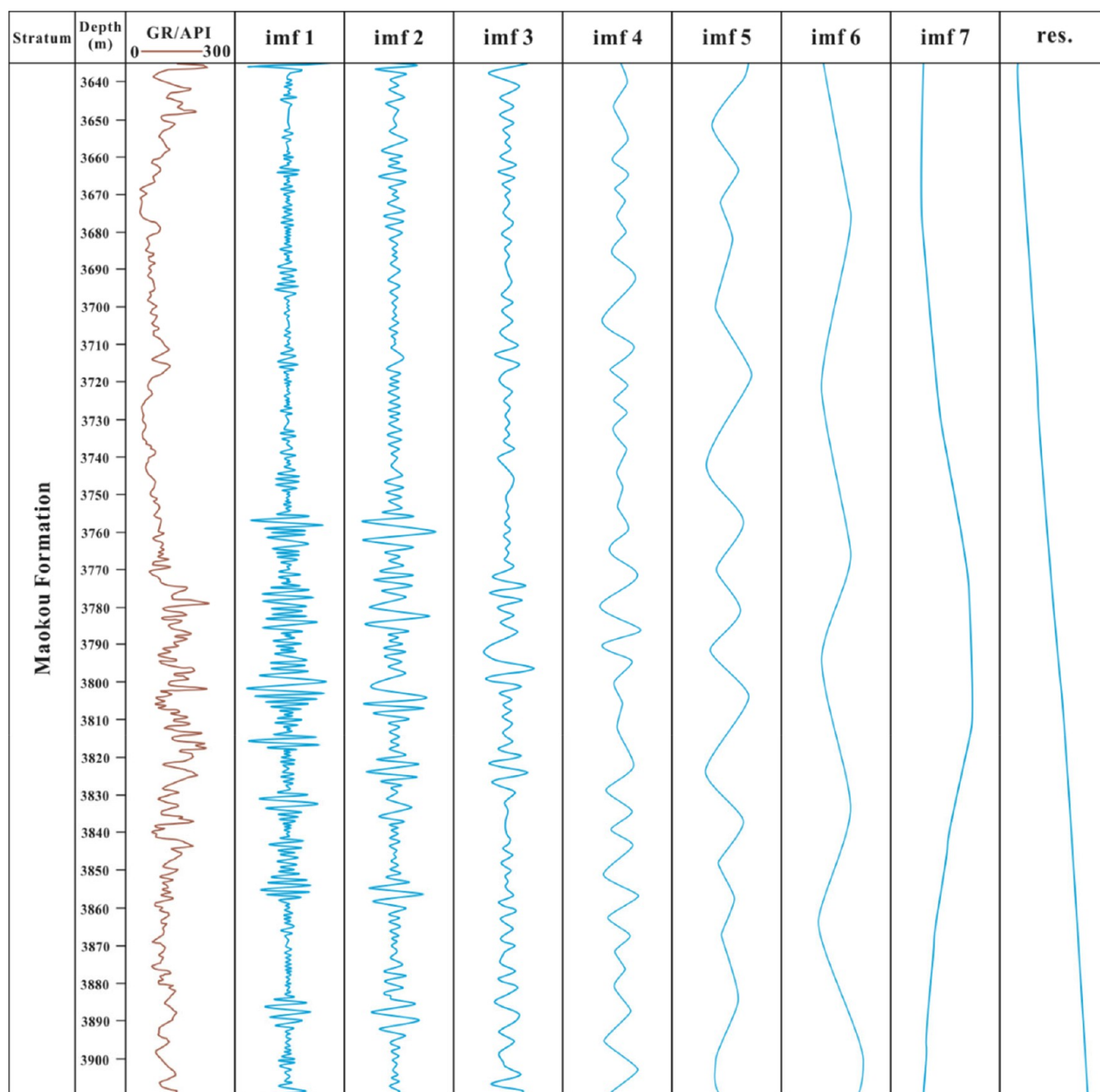
Figure 6. EMD analysis results of GR logging data of the Maokou Formation in LS3.

formation was not denuded.[30] Therefore, the Maokou Formation in this area retained a relatively complete sedimentary cycle. Here, we selected four wells for EMD analysis. Among them, YH1 and JS1 were located between Chongqing and Fuling, and wells FS1 and FS2 were located in eastern Sichuan. As shown in Figure 9, the imf.3 components of YH1 and JS1 identified 77 e_3 cycles, while the numbers of cycles identified in FS1 and FS2 were 49 and 56, respectively, which

Table 5. Cycle Number of Milankovitch Cycles and the imf Curve

well	thickness of Maokou Formation (m)	number of e_2 cycles	number of e_3 cycles	number of o_1 cycles	number of o_2 cycles	number of cycles (imf.3)	number of cycles (imf.4)
LS1	240.625	36.82	48.85	98.42	132.10	49	24
LS2	264.625	46.84	61.39	126.76	159.57	62	33
LS3	272.000	42.43	56.30	117.78	145.52	56	28
X14	235.000	47.00	62.04	130.43	167.56	61	31
T15	218.875	54.06	72.45	151.46		74	34
XM1	224.500	54.78	67.57	148.39		67	31
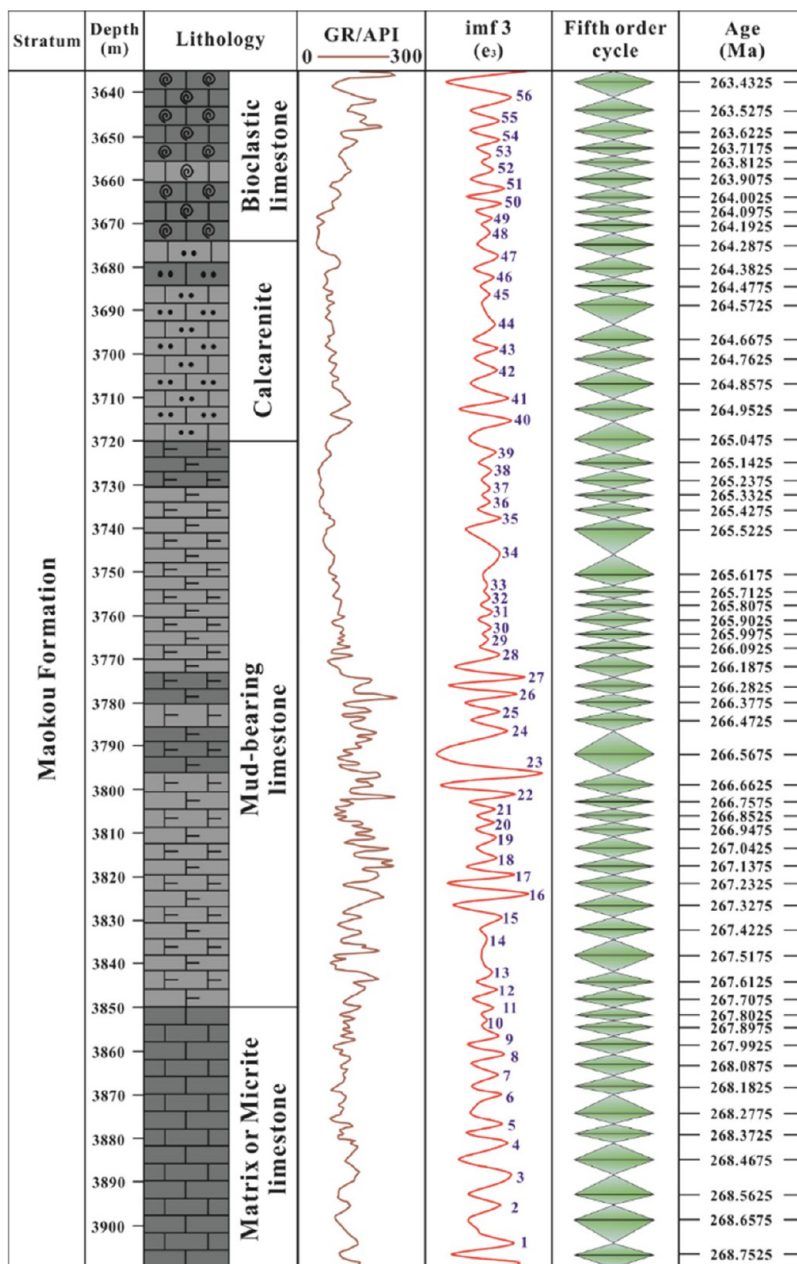
Figure 7. Astronomical age scale of the Maokou Formation in LS3.

were in agreement with the research result of Jiang et al. Therefore, we believe that the area between Chongqing and Fuling suffered the weakest denudation during the Dongwu movement, and the remaining stratum is relatively complete with 77 e_3 cycles.

Therefore, we can calculate the eroded thickness based on the number of missing e_3 cycles and the average cycle thickness. The

calculation results based on the average cycle thickness are shown in Table 6. The eroded thickness (method 1) of the six wells was in the range of 8.87 to 102 m, with an average of 60.59 m. The eroded thickness of LS3 was the largest, while that of T15 was the smallest.

3.5.2. Calculating the Eroded Thickness Based on the Missing Formation Deposition Rate. The relationship between
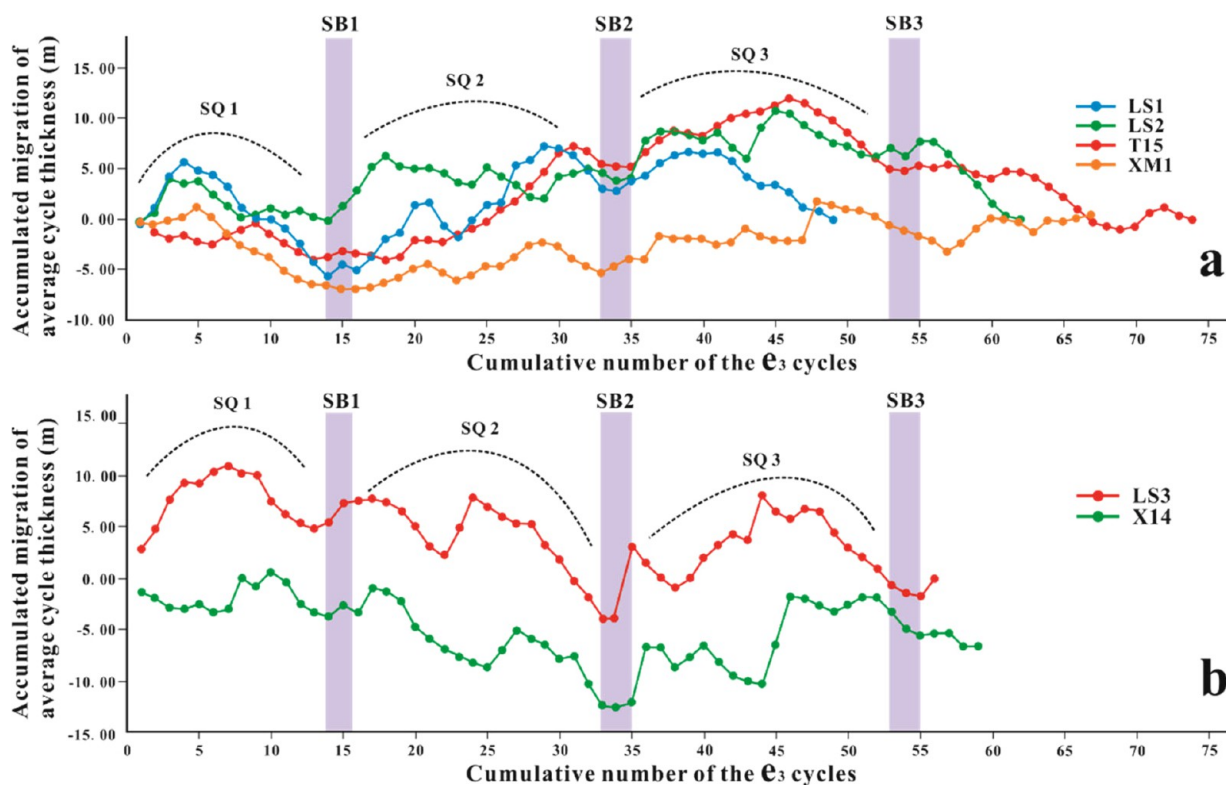
Figure 8. (a) Fischer plots and three-order cycle division of LS1, LS2, T15, and XM1. (b) Fischer plots and three-order cycle division of LS3 and X14.

the primary rock types of each e_3 cycle and the deposition rate was analyzed. Notably, when the thickness of two types of rocks exceeded 30%, the data were discarded (Figure 10). The factors affecting the deposition rate of carbonate rocks are more complex than those of clastic rocks. Sea-level location, marine water flu, paleogeomorphology, paleo-water temperature, paleo-salinity, local material sources, and other factors may affect the deposition rate of carbonate rocks.[41,42] Obviously, when the shale content is greater than 10%, the deposition rate and the shale content show a weak positive correlation (R^2 is between 0.2596 and 0.4510). While when the mud content is less than 10%, there is no obvious correlation. This shows that when the shale content is relatively high, the influence of sea-level changes (related to changes in shale content) on the deposition rate of limestone is more obvious than when the shale content is low.

In addition, different types of rocks exhibit different ranges of sedimentation rates. The deposition rate of bioclastic limestone was relatively low, concentrated in 2.12−5.36 cm/ka, with an average of 3.30 cm/ka. The deposition rate of calcarenite was 2.27−5.25 cm/ka, with an average of 4.09 cm/ka. The sedimentation rate of argillaceous limestone was relatively high, in the range of 3.18−5.77 cm/ka, with an average of 4.37 cm/ka. The variation range of deposition rate of common limestone and mud-bearing limestone was close. Generally, the upper limits of the sedimentation rate from large to small were argillaceous limestone, common limestone (and calcarenite), mud-bearing limestone, and bioclastic limestone, whereas the lower limits from large to small were argillaceous limestone, bioclastic limestone, common limestone (and calcarenite), and mud-bearing limestone.

There were three lithological combinations (from bottom to top) in the Maokou Formation of six wells (Figure 11). The first type was marl-bearing limestone (or common limestone)−argillaceous limestone (or mud-bearing limestone)−marl-bearing limestone (or common limestone)−bioclastic limestone; LS1, LS2, and T15 belonged to this type. The second type was marl-bearing limestone (or common limestone)−argillaceous limestone (or mud-bearing limestone)−calcarenite−bioclastic limestone, including LS3 and X14. The third type was common limestone−mud-bearing limestone−bioclastic limestone−common limestone, such as XM1. As such, the missing formations of LS1, LS2, T15, LS3, and X14 were bioclastic limestones, while the missing formations of XM1 were common limestones. Based on Figure 10, the deposition rate of the same rock type in different wells was different; hence, we used an average deposition rate of a similar type of rock in the same well as the deposition rate of the missing formation (Table 6).

Therefore, we can calculate the eroded thickness based on the number of missing e_3 cycles and the average deposition rate of the missing strata. The eroded thickness based on the missing formation deposition rate (method 2) of the six wells was in the range of 7.38 to 91.97 m with an average of 49.92 m (Table 6). LS3 experienced the strongest denudation, whereas T15 had the smallest eroded thickness.

3.5.3. Calculating the Eroded Thickness Based on the Fischer Curve Fitting Formula. Notably, the Fischer plot revealed the periodic variation of the accommodating space. Therefore, the fitting equation was used to represent the changing trend of the Fischer curve. We attempted to fit the Fischer curve using different types of functions and discovered that the polynomial of the sine function showed a similar curve shape, and the fitting degree was high (Figure 12). Liu et al. established the wave equation of the relationship between the deposition rate and the strata age of the Sanshui Basin from 140 to 0 Ma.[43] The wave equation was also a polynomial of sine function in form, indicating that the Fischer curve fitting formula was reasonable.
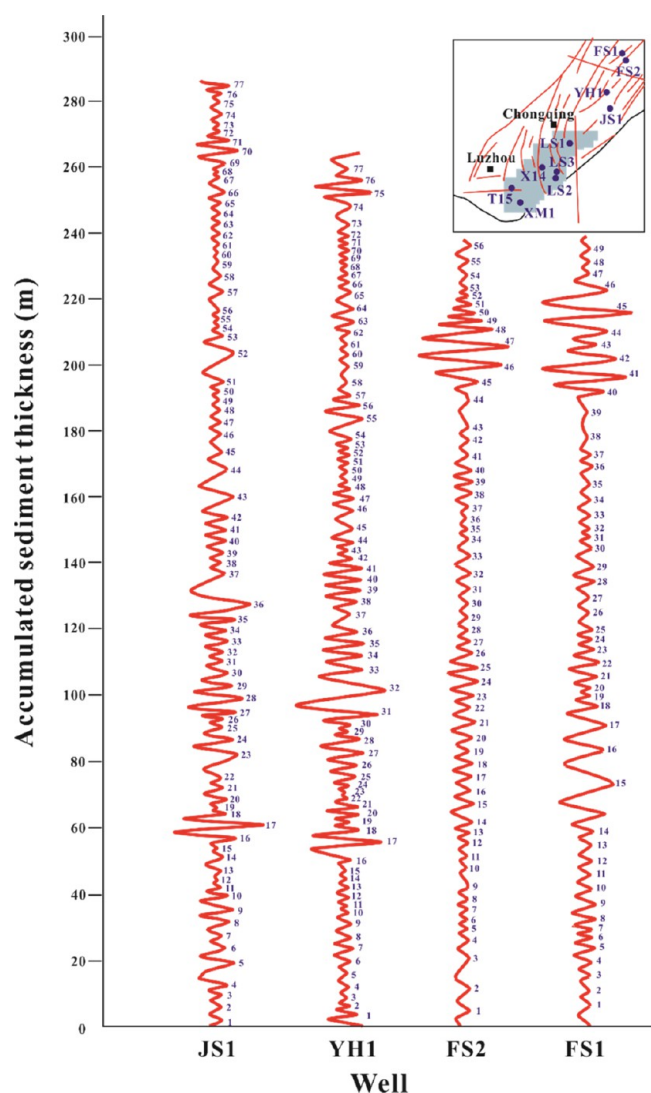
Figure 9. Component imf.3 and number of e_3 cycles of the Maokou Formation of the four wells (JS1, YH1, FS2, and FS1).

Therefore, the shape of the Fischer curve of the missing formation was predicted using the fitting formula. According to the calculation result of the Fischer curve fitting formula method (Table 6, method 3), the eroded thickness was in the range of 9.13−83.82 m, and the average was 54.33 m. The eroded thicknesses of LS3 and T15 were the largest and smallest, respectively.

3.5.4. Calculating the Eroded Thickness Based on Seismic Data. Based on the Fischer plots of the six wells, three third-order cycles were identified in the remaining strata of the Maokou Formation, and the boundaries between them were approximately the 15th, 34th, and 54th e_3 cycles (Figure 8). As shown in Figure 11, during the 31st to 36th e_3 cycles, the shale content significantly decreased, which was believed to be related to the reduction of the accommodating space in the later stage of the SQ2. The large changes in shale content can be identified by seismic signals. According to 2D seismic data, there were three or two positive phase seismic reflection in-phase axes in the Maokou Formation, with moderate reflection intensity and satisfactory continuity. By analyzing the relationship between the seismic reflection in-phase axis and the lithological interface, it was found that the sequence boundary SB_2 corresponded to the first positive phase seismic reflection in-phase axis below the top of the Maokou Formation (Figure 13). Therefore, the stratum from the bottom to the seismic reflection in-phase axis corresponding to SB2 comprised 34 e_3 cycles, while the remaining stratum contained 43 e_3 cycles.

According to the above analysis, we can calculate the eroded thickness based on seismic data. The advantage of this method is that it calculates the eroded thickness without wells. The formation thickness can be calculated by time-depth conversion. The eroded thickness (method 4) of the six wells was in the range of 15.23 to 105.14 m, with an average of 49.94 m. The eroded thickness of LS3 was the largest, while that of XM1 was the smallest.

3.5.5. Comparison and Analysis of Calculation Results. After analyzing the calculation results of the four methods, the maximum eroded thickness was less than 105 m (Table 6), suggesting that the study area was on the obliquity of the paleo-uplift during the Dongwu movement period, not the area with the strongest tectonic uplift, which was consistent with the research result of Jiang et al.[30] There were two major differences in the calculation results of different methods. First, the calculation results of methods 1, 3, and 4 showed that the eroded thickness of LS1 was close to that of LS3, while method 2 showed that the eroded thickness of LS1 was significantly smaller than that of LS3 (Figure 14). Comparing the core features 20 m below the top surface of the Maokou Formation, collapsed breccias and small karst caves were developed in LS3, while only high-angle dissolution fractures were developed in LS1 (Figure 15), indicating that the denudation experienced by LS3 was more intense. Therefore, the calculation method based on the actual formation deposition rate was relatively more precise.

Table 6. Eroded Thickness Calculation Results of Different Methods[a]

					eroded thickness (m)			
well	lithology of the missing formation	deposition rate of the missing formation (cm/ka)	number of missing cycles	thickness of SQ1 and SQ2 (m)	method 1	method 2	method 3	method 4
LS1	bioclastic limestone	3.73	28	173.91	90.72	52.44	77.50	106.45
LS2	bioclastic limestone	4.02	15	150.44	64.02	57.29	44.97	76.08
LS3	bioclastic limestone	4.61	21	169.23	102.00	91.97	83.82	111.26
X14	bioclastic limestone	3.60	17	116.97	66.58	58.14	71.44	29.90
T15	bioclastic limestone	2.59	3	105.37	8.87	7.38	9.13	19.76
XM1	common limestone	3.40	10	108.25	33.51	32.30	39.16	20.65

[a]Method 1: calculating based on the average cycle thickness; method 2: calculating based on the average deposition rate of missing formation; method 3: calculating based on the fitting formula of the Fischer curve; method 4: calculating based on the 2D seismic data.
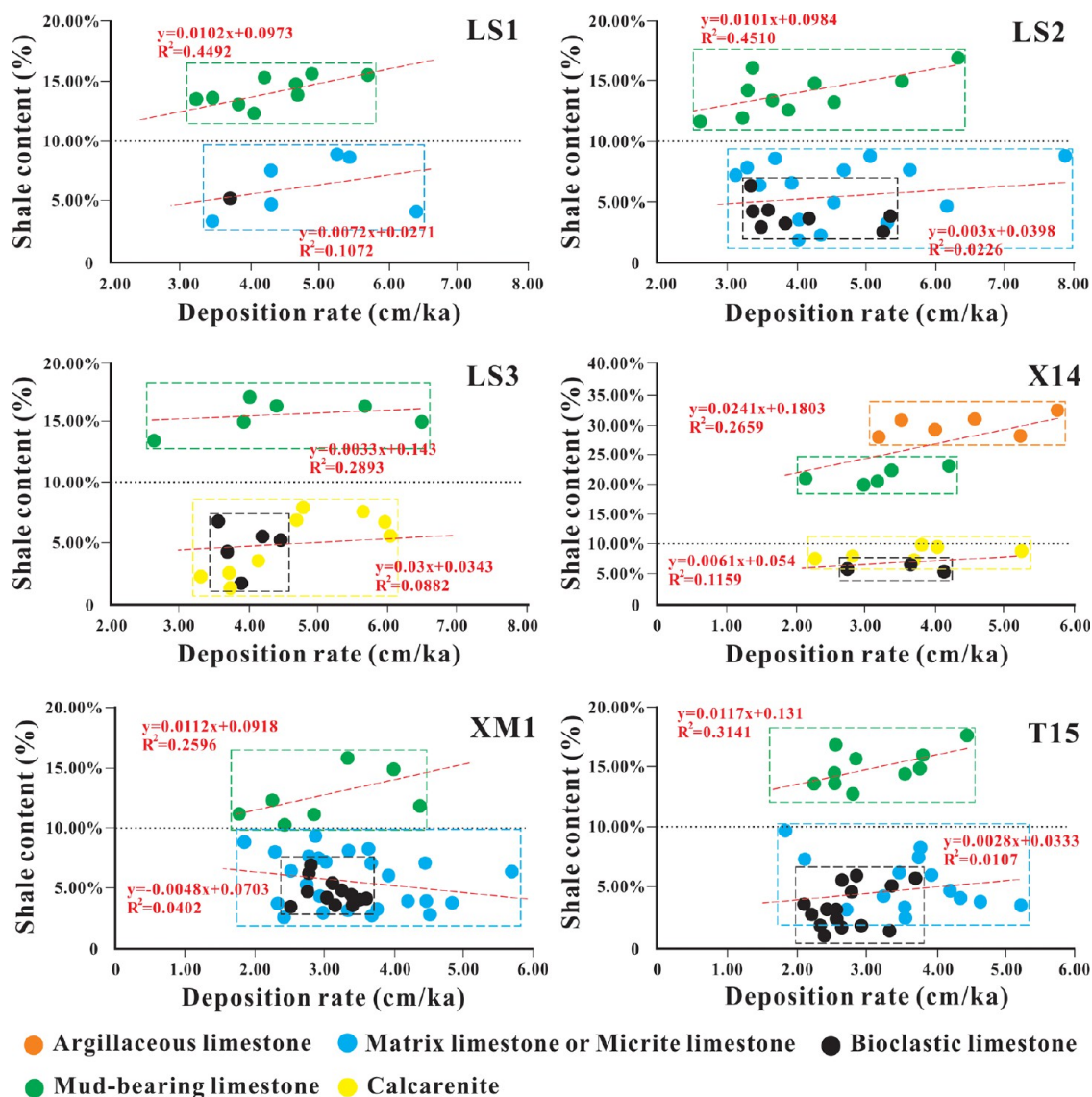
Figure 10. Relationship between lithology and deposition rate of the Maokou Formation.

Additionally, based on the calculation results of methods 1, 2, and 3, the eroded thickness of XM1 was significantly greater than that of T15, while the calculation result of method 4 showed that the eroded thicknesses of XM1 and T15 were close. Due to the lack of core samples, we only analyzed where the calculation result was more reasonable based on the calculation principle. Method 1 took the average cyclic thickness (or average deposition rate) of the residual strata as that of the missing strata. Method 2 regarded the deposition rate of similar lithological strata as that of the missing strata. Method 3 calculated the eroded thickness based on the periodic change of the accommodating space of the residual strata. Method 4 considered the average cycle thickness (or average deposition rate) of systems SQ1 and SQ2 as that of the missing formation. According to Figures 10 and 11, the lithology of the missing formation in XM1 was common limestone (matrix limestone or micrite limestone), while the other five wells were bioclastic limestone. The deposition rate of common limestone was significantly higher than that of mud-bearing limestone, while that of bioclastic limestone was significantly smaller than the others. The main lithologies of the system tract I and system tract II were common limestone and mud-bearing limestone (or

argillaceous limestone), respectively. Therefore, the calculation result of method 4 caused the eroded thickness of XM1 to be smaller, while the other five wells became larger.

In summary, the eroded thicknesses of the six wells from large to small were LS3, X14, LS2, LS1, XM1, and T15. Among the four methods, method 2 was relatively accurate. Among the four calculation methods, the accuracy of method 4 is relatively low. According to Figure 14, in areas with strong denudation, the calculation results of method 4 are relatively large, and in areas with weak denudation, the calculation results are concentrated in a certain interval. In addition, it should be noted that the accuracy of method 4 is also affected by seismic data quality and data reading errors. We only recommend using this method in research areas that lack logging data and have relatively high seismic data quality.

3.5.6. Eroded Thickness Distribution of the Maokou Formation in Southeastern Sichuan. To study the eroded thickness distribution of the Maokou Formation in southeastern Sichuan, a total of 109 virtual wells (with an average interwell distance of about 12.31 km) were set on the 43 2D seismic survey lines in the study area (Figure 16).
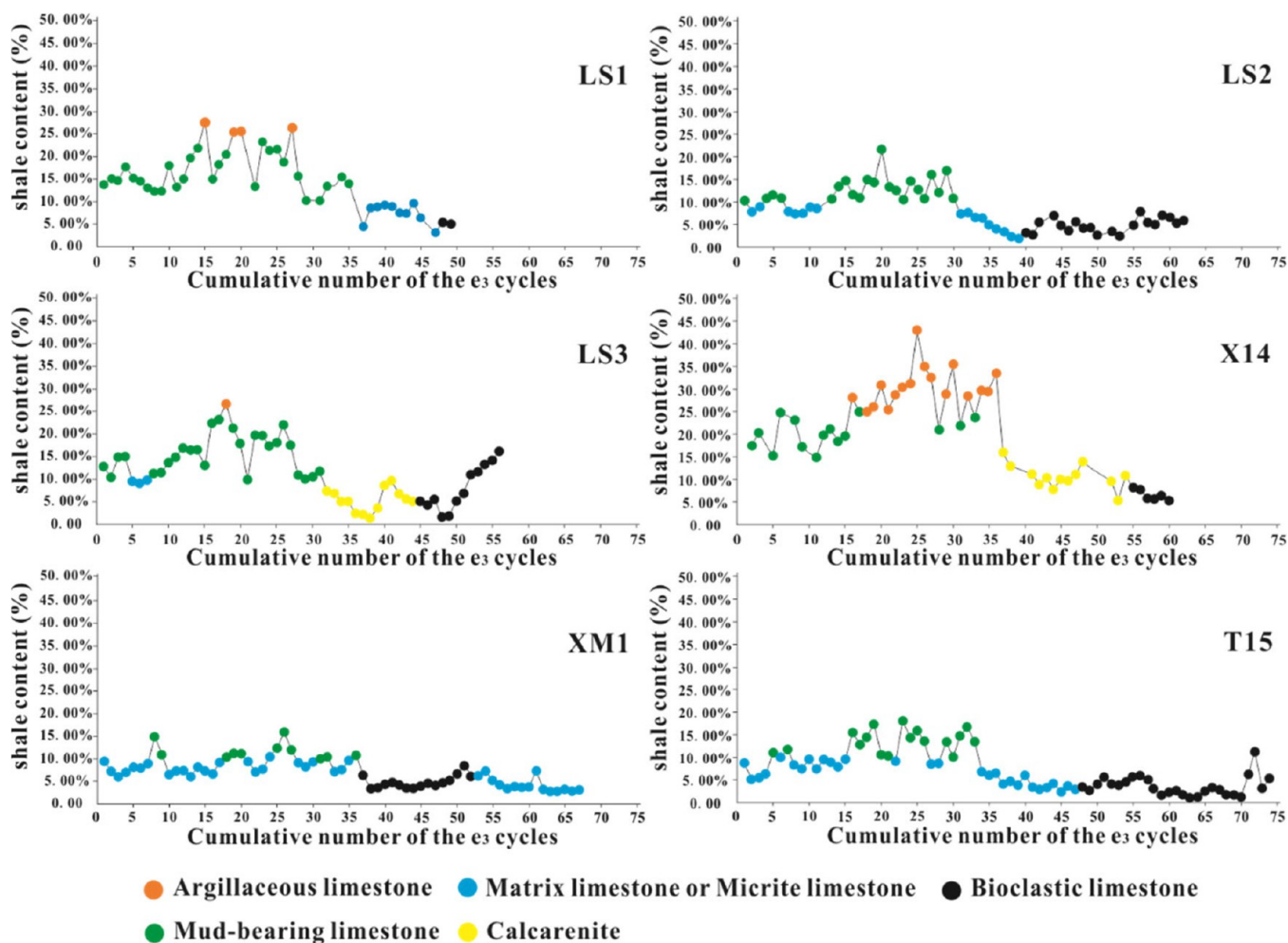
Figure 11. Shale content and dominant lithology of each e₃ cycle.

Finally, we drew a contour map of the eroded thickness of the Maokou Formation in southeastern Sichuan. The data of the six wells were based on method 2, and the data of 109 virtual wells were calculated by method 4. The results revealed that the eroded thickness of the Maokou Formation in the study area varied within the range of 0−140 m, while the area north of LS1 had the smallest eroded thickness (<40 m), indicating that the area was low in the structural position during the Dongwu movement. The southern and western parts of X14 had the largest eroded thickness, which were considered close to the center of the paleo-uplift. The eroded thickness in other areas varied within the range of 40−100 m, with high and low values alternately appearing, showing the characteristics of differential structural uplift.

4. CONCLUSIONS

(1) Based on the spectrum analysis and continuous wavelet transform method, the dominant frequency signals corresponding to the middle eccentricity (e₂), short eccentricity (e₃), long obliquity (o₁), and short obliquity (o₂) were identified from the GR logging data of the Maokou Formation of the six wells in southeast Sichuan. The cycle number of the component imf.3 was similar to the number of short eccentricity (e₃) cycles, which was used to establish the astronomical age scale.

(2) The Fischer curves of the six wells were divided into two shapes, i.e., V-shaped and inverted V-shaped, which might be related to local structural uplift. The 1st to 54th e₃ cycles of the residual strata contained three complete third-order cycles, and the boundaries were the 15th, 34th, and 54th e₃ cycles.

(3) The area between Chongqing and Fuling suffered the weakest denudation during the Dongwu movement, and the remaining stratum was relatively complete, comprising 77 e₃ cycles.

(4) When the shale content was greater than 10%, the sedimentation rate of the Maokou Formation became mainly affected by sea-level changes; when the shale content was less than 10%, the changes in the sedimentation rate might be mainly affected by factors including paleo-salinity and paleo-water temperature. The deposition rate of bioclastic limestone in the Maokou Formation in the study area was the smallest, varying within the range of 2.12−5.36 cm/ka with an average of 3.30 cm/ka. The deposition rate of argillaceous limestone was the largest, concentrated in 2.27−5.25 cm/ka with an average of 4.09 cm/ka. Moreover, the deposition rate of the same lithology in different wells was different.

(5) The eroded thickness at the top of the Maokou Formation in southeastern Sichuan was calculated by four methods. Among them, the correlation between the calculation results of the missing formation deposition rate method
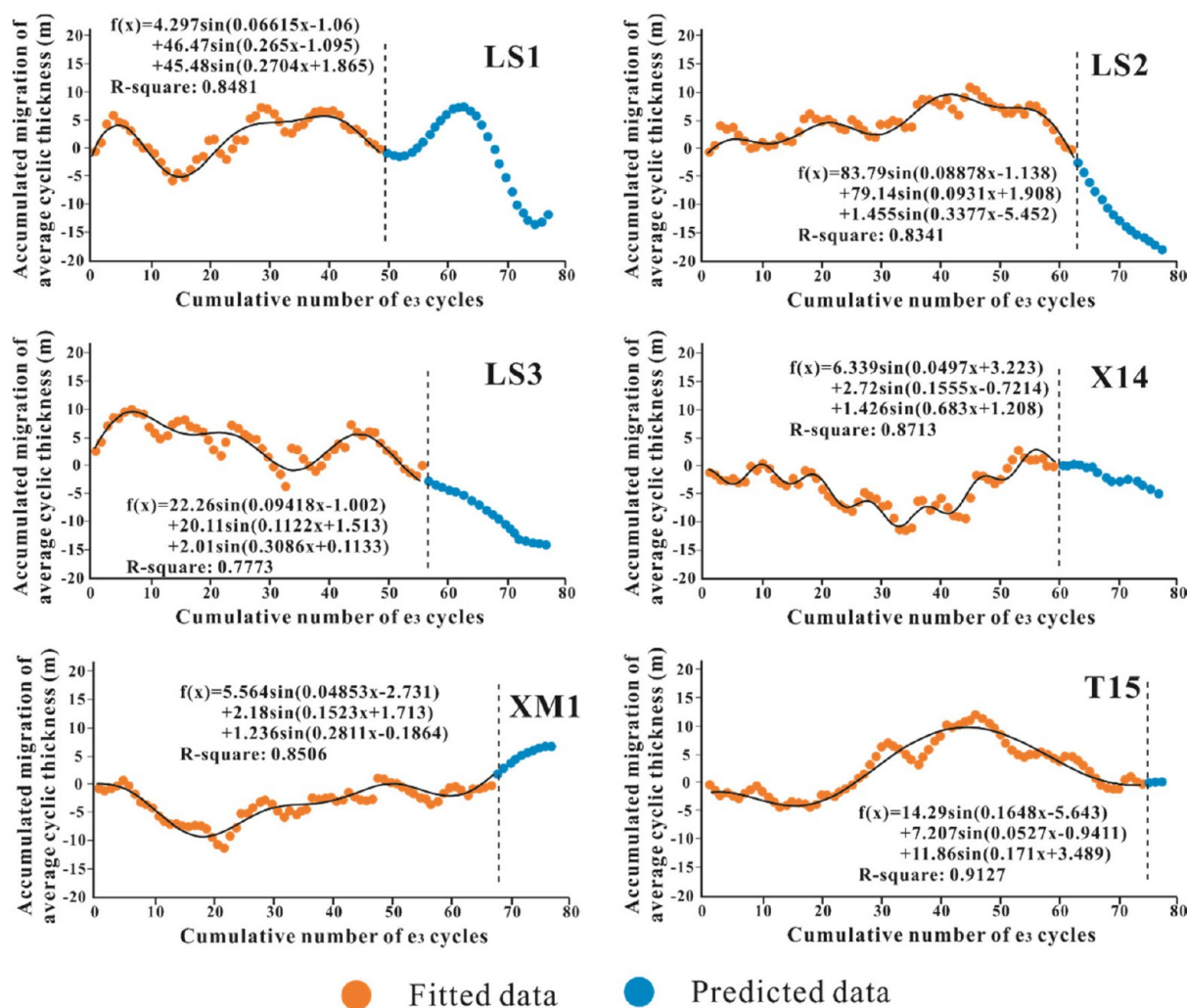
Figure 12. Calculation of the eroded thickness based on the Fischer curve fitting formula method.

and the karst development characteristics was satisfactory, and the calculation results were regarded as the most reasonable. The calculation results of the average cycle thickness method and the Fischer curve fitting curve method were similar. The accuracy of the seismic sequence method was relatively low but can be used without the constraints of well data.

(6) The southeastern Sichuan area was a paleo-uplifted obliquity during the Dongwu movement. The erosion thickness of the Maokou Formation was 0−140 m. The area west and south of X14 had the largest eroded thickness, while the area north of LS1 experienced the weakest denudation.

5. DATA AND COMPUTATIONAL METHODS

5.1. Basic Data. This study used the geologic and gamma (GR) logging data obtained from six wells. The locations of the six wells are shown in Figure 1. The geologic data comprise stratigraphic data and lithology. It is noteworthy that the upper part of the Maokou Formation of LS1 was staggered by a reverse fault, and the thickness of the Maokou Formation in the upper wall was 46.78 m. To ensure the accuracy of astronomical period identification, data only situated in the footwall were selected. Gamma (GR) logging data had a higher longitudinal resolution and a sampling interval of 0.125 m, which sensitively reflected

the cyclicity changes of different lithology combinations. As such, GR logging data were selected as the basic data to identify astronomical cycles. Before the cycle analysis, the GR logging data were preprocessed to remove ultralow frequency and ultrahigh frequency signals and eliminate errors caused by noise and environmental factors. In addition, this work used 43 2D seismic lines with a total length of about 2100 km. The location of the lines is listed in Figure 16. All the above data were provided by Sinopec Exploration Company, Chengdu, Sichuan, China.

5.2. The Computational Methods of the Eroded Thickness Based on the Average Cycle Thickness. The eroded thickness was calculated based on the average cycle thickness by the following formula

$$H_d = (N - n) \times (H/n) \tag{3}$$

where H_d represents the eroded thickness (m), N represents the total number of e_3 cycles recorded by the sedimentation of the Maokou Formation, namely, 77, and H represents the residual formation thickness (m).

5.3. The Computational Methods of the Eroded Thickness Based on the Missing Formation Deposition Rate. The eroded thickness based on the missing formation deposition rate was calculated by the following formula
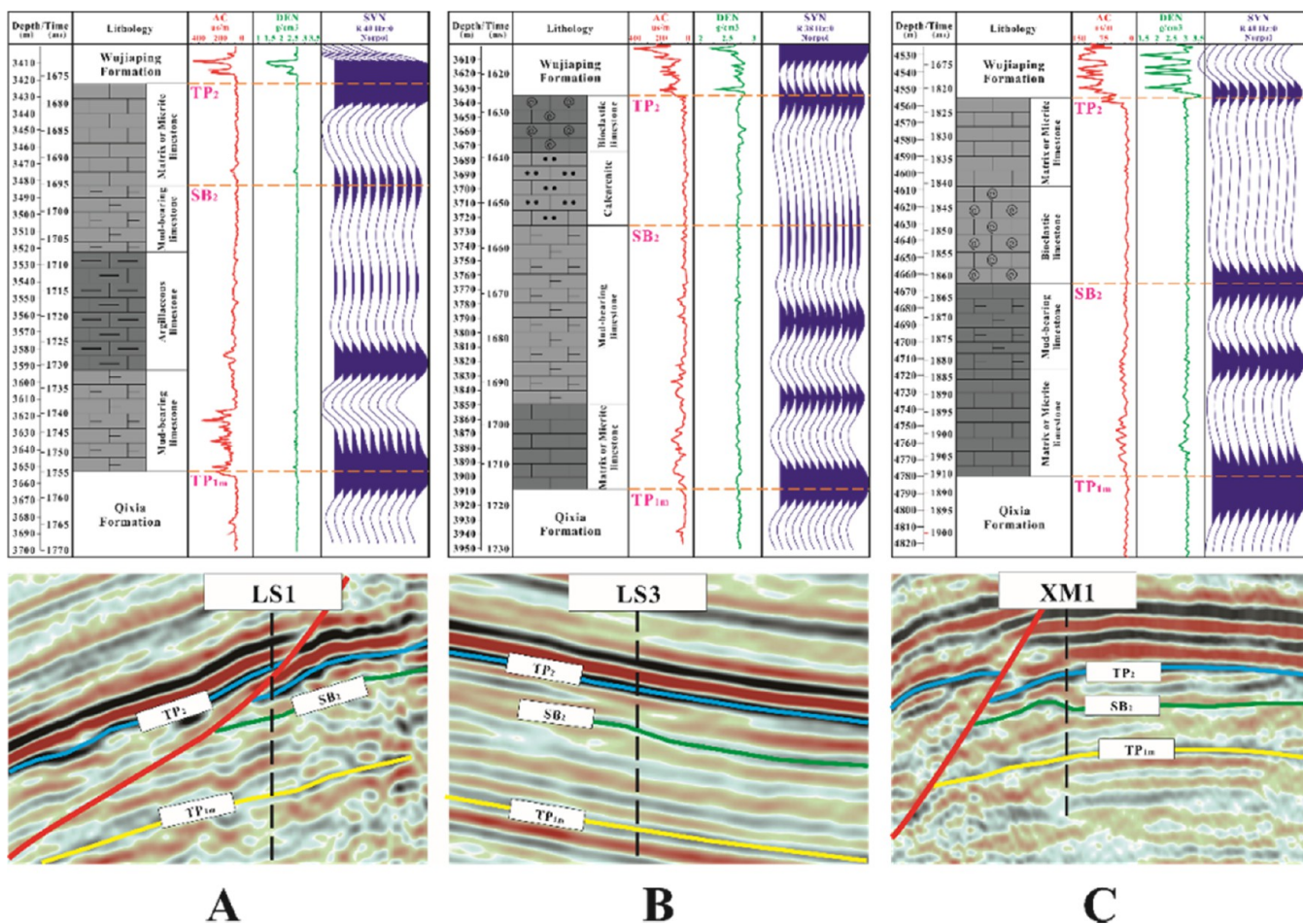
Figure 13. Correspondence between the boundary of the third-order cycle and the seismic reflection in-phase axis. (A, B, and C in the figure correspond to LS1, LS3, and XM1, respectively.)
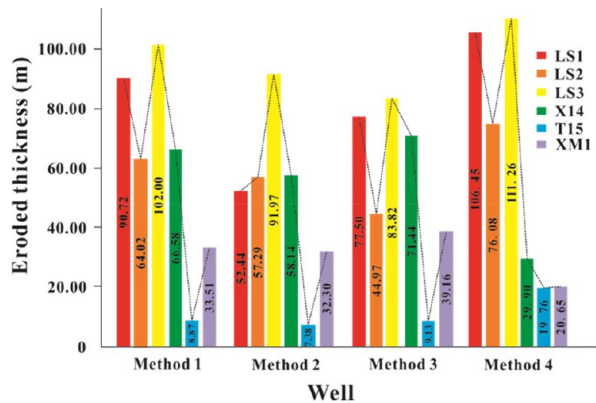
Figure 14. Eroded thickness calculation results of four methods (method 1: calculating based on the average cycle thickness; method 2: calculating based on the average deposition rate of missing formation; method 3: calculating based on the fitting formula of the Fischer curve; method 4: calculating based on the 2D seismic data).

$$H_d = (N - n) \times T \times V_m \qquad (4)$$

where T represents the e_3 cycle period, namely, 95 kyr, and V_m represents the average deposition rate of the missing formation (m/kyr).

5.4. The Computational Methods of the Eroded Thickness Based on the Fischer Curve Fitting Formula.
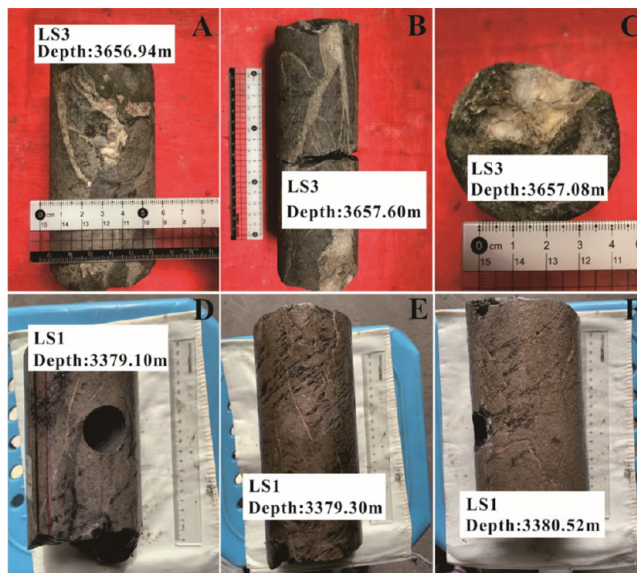
Figure 15. (A−F) Core features of the Maokou Formation in LS3 and LS1 (about 20 m below the top surface).

The eroded thickness based on the Fischer curve fitting formula was calculated by the following formula
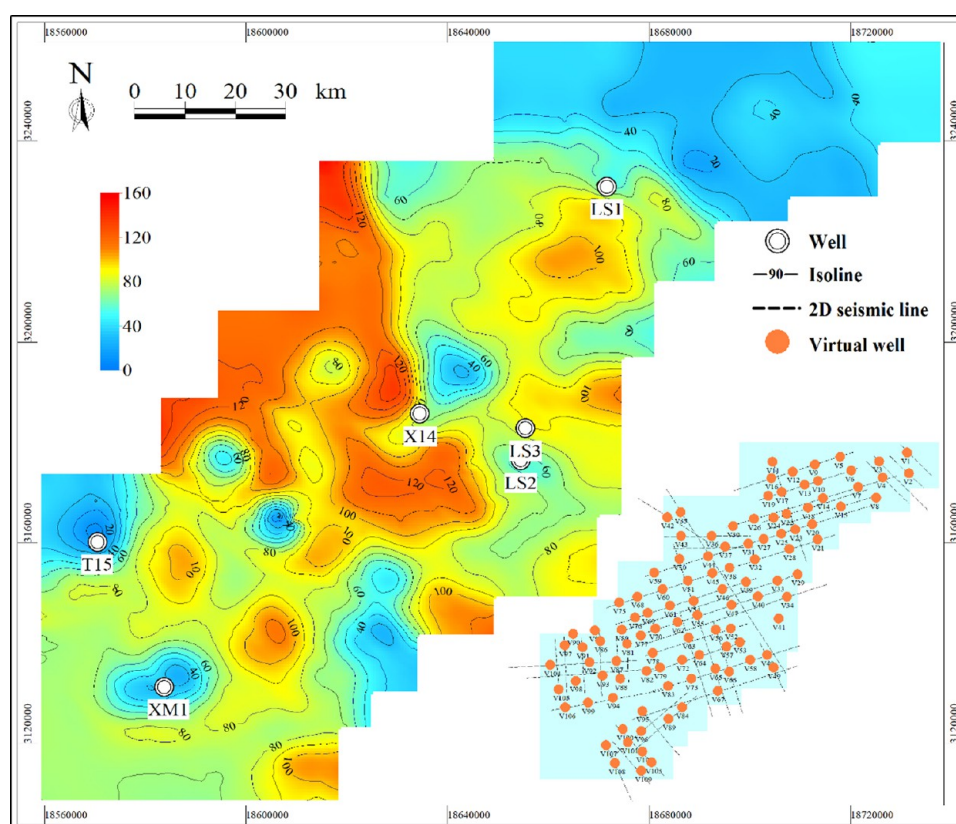
Figure 16. Contour map of eroded thickness of the Maokou Formation in southeastern Sichuan.

$$H_d = \sum_{i=n}^{N} [Y(x+1) - Y(x) + h_{ac}] \tag{5}$$

where $Y(x)$ represents the fitting formula.

5.5. The Computational Methods of the Eroded Thickness Based on Seismic Data. The eroded thickness based on seismic data was calculated according to the following formula

$$H_d = H' + 43 \times H'/34 - H \tag{6}$$

where H' represents the formation thickness of SQ1 and SQ2 (m).

AUTHOR INFORMATION

Corresponding Author

Wenlong Ding − *School of Energy Resources, China University of Geosciences, Beijing 100083, P. R. China;* ⊙ orcid.org/ 0000-0002-5328-7629; Phone: +86 10 82320629; Email: dingwenlong2006@126.com; Fax: +86 10 82326850

Authors

Siyu Shi − *School of Energy Resources, China University of Geosciences, Beijing 100083, P. R. China;* ⊙ orcid.org/0000-0003-2732-6118

Gang Zhao − *SINOPEC Petroleum Exploration and Production Research Institute, Beijing 100083, P. R. China*

Zikang Xiao − *School of Energy Resources, China University of Geosciences, Beijing 100083, P. R. China*

Yuntao Li − *School of Energy Resources, China University of Geosciences, Beijing 100083, P. R. China*

Baocheng Jiao − *School of Energy Resources, China University of Geosciences, Beijing 100083, P. R. China*

Complete contact information is available at:
https://pubs.acs.org/10.1021/acsomega.0c05989

Notes

The authors declare no competing financial interest.

REFERENCES

(1) Wang, F.-h.; Jiang, Z.-x. Promotion of strata uplift and erosion to hydrocarbon accumulation. *J. Southwest Pet. Inst.* **2008**, *30*, 37−40.

(2) Sun, Y. J.; Zhou, L. F. Reflections on two problems of the weathering crust karst dolomite reservoirs. *Unconv. Oil Gas* **2019**, *6*, 106−113.

(3) Gao, F. Prediction of carbonate erosion flutes, fracture and cavity by seismic forward modeling and attributes: A case study of Majiagou Formation in Ganquan Area of Ordos Basin. *Unconv. Oil Gas* **2019**, *6*, 25−32.

(4) Magara, K. Thickness of removed sedimentary rocks, paleopore pressure, and paleotemperature, southwestern part of Western Canada Basin. *AAPG Bull.* **1976**, *60*, 554−566.

(5) Dow, W. G. Kerogen studies and geological interpretations. *J. Geochem. Explor.* **1977**, *7*, 79−99.

(6) Van Hinte, J. E. Geohistory analysis-application of micro-paleontology in exploration geology. *AAPG Bull.* **1978**, *62*, 201−222.

(7) Guidish, T. M.; Kendal, C. S. C.; Lerche, I.; Toth, D. J.; Yarzab, R. F. Basin evaluation using burial history calculations: an overview. *AAPG Bull.* **1985**, *62*, 92−105.

(8) Laslett, G. M.; Green, P. F.; Duddy, I. R.; Gleadow, A. J. W. Thermal annealing of fission tracks in apatite. 2. A quantitative analysis. *Chem. Geol.* **1987**, *65*, 1−13.

(9) Li, M. C.; Li, W. A study of natural gas diffusion by equilibrium concentration-A new method for diffusion quantitative modelling. *Nat. Gas Ind.* **1996**, *16*, 1−5.

(10) Abels, H. A.; Aziz, H. A.; Krijgsman, W.; Smeets, S. J. B.; Hilgen, F. J. Long-period eccentricity control on sedimentary sequences in the continental Madrid Basin (middle Miocene, Spain). *Earth Planet. Sci. Lett.* **2010**, *289*, 220−231.

(11) Hilgen, F. J.; Kuiper, K. F.; Lourens, L. J. Evaluation of the astronomical time scale for the Paleocene and earliest Eocene. *Earth Planet. Sci. Lett.* **2010**, *300*, 139−151.

(12) Wang, H.; Shi, Z.; Zhao, Q.; Liu, D.; Sun, S.; Guo, W.; Liang, F.; Lin, C.; Wang, X. Stratigraphic framework of the Wufeng-Longmaxi shale in and around the Sichuan Basin, China: Implications for targeting shale gas. *Energy Geosci.* **2020**, *1*, 124−133.

(13) Xia, S.; Lin, C.; Du, X.; Jia, D.; Ahmad, N.; Zhang, Z.; Gao, L.; Zhu, Y. Correspondences among lacustrine fluctuations, climate changes and the Milankovitch cycles in the Paleogene through tracking onlap points and correlating palaeontology in Liaozhong Depression, Bohai Bay Basin, NE China. *Geol. J.* **2020**, *55*, 6527−6543.

(14) Zhao, J.; Cao, Q.; Fu, X. D.; Zhang, F. F.; Qin, G. Y.; Yan, W. W. Recovery of denuded strata thickness based on Milankovitch astronomical cycles: a case study of Qingshankou formation in X oilfield, Songliao Basin. *Pet. Geol. Exp.* **2018**, *40*, 260−267.

(15) Guo, Y.; Tang, L. J.; Yue, Y.; Chen, G.; Long, Y.; Xie, X. T. Application of cycle analysis method to estimate the denuded strata thickness: a case study of Middle-Lower Ordovician Yingshan formation of the eastern Yubei area, Tarim Basin. *J. China Univ. Min. Technol.* **2015**, *44*, 664−672.

(16) Yao, Y. M.; Xu, X. H.; Liu, C. R.; Tan, C. P.; Luo, J. Q.; Zhu, J. X. Calculation of denudation amount with Milankovitch cycle method: a case study in Biyang Sag. *Pet. Geol. Exp.* **2011**, *33*, 460−467.

(17) Grin, E.; Schaller, M.; Ehlers, T. A. Spatial distribution of cosmogenic [10]Be derived denudation rates between the Western Tian Shan and Northern Pamir, Tajikistan. *Geomorphology* **2018**, *321*, 1−15.

(18) Dai, X.; Zhang, M.; Jiang, Q.; Feng, Z. Karst reservoirs seismic prediction of Lower Permian Maokou Formation in central Sichuan Basin, SW China. *Pet. Exp. Dev.* **2017**, *44*, 79−88.

(19) Huang, S.; Jiang, Q.; Feng, Q.; Wu, Y.; Lu, W.; Su, W.; Chen, X.; Ren, M.; Peng, H. Type and distribution of Mid-Permian Maokou Formation karst reservoirs in southern Sichuan Basin, SW China. *Pet. Exp. Dev.* **2019**, *46*, 293−300.

(20) Su, W.; Hu, S.; Jiang, Q.; Zhang, J.; Huang, S.; Jiang, H.; Shi, S.; Wang, K.; Chen, X.; Zhang, H.; Ren, M. Sedimentary responses to the Dongwu movement and the influence of the Emeishan mantle plume in Sichuan Basin, Southwest China: significance for petroleum geology. *Carbonates Evaporites* **2020**, *35*, 108.

(21) Tang, D.; Xiao, D.; Tan, X.; Li, H.; Xie, J.; Liu, H.; Yang, X.; Zhang, B. Restoration of paleokarst landform and its geological significance: A case from Middle Permian Maokou Formation in Northwestern Sichuan Basin. *Pet. Exp. Dev.* **2016**, *43*, 751−758.

(22) Xiao, D.; Tan, X. C.; Xi, A. H.; Liu, H.; Shan, S. J.; Xia, J. W.; Cheng, Y.; Lian, C. B. An inland facies-controlled eogenetic karst of the carbonate reservoir in the Middle Permian Maokou Formation, Southern Sichuan Basin, SW China. *Mar. Pet. Geol.* **2016**, *72*, 218−233.

(23) Ge, L.; Tong, K.; Meng, Z.; Zhu, Z.; Zhu, X. Construction of an efficient development mode for buried-hill fractured reservoirs in Bohai Bay. *Adv. Geo-Energy Res.* **2020**, *4*, 162−172.

(24) Liu, H.; Tang, Y.; Tan, X.; He, B.; Tang, S.; Zhou, Y.; Lin, B. Paleogeomorphological reconstruction and geological implications of the weathered-crust karst on the top of the Middle Triassic Leikoupo

Formation in the Longgang area, Sichuan Basin, China. *Energ. Explor. Exploit.* **2017**, *36*, 727−742.

(25) Wu, G.; Lin, C.; Yang, H.; Liu, J.; Liu, Y.; Li, H.; Yang, X.; Jiang, J.; He, Q.; Gao, D. Major unconformities in the Mesozoic sedimentary sequences in the Kuqa−Tabei region, Tarim Basin, NW China. *J. Asian Earth Sci.* **2019**, *183*, 103957−103916.

(26) Zhang, Y.; Tan, F.; Qu, H.; Zhong, Z.; Liu, Y.; Luo, X.; Wang, Z.; Qu, F. Karst monadnock fine characterization and reservoir control analysis: A case from Ordovician weathering paleokarst reservoirs in Lungu area, Tarim Basin, NW China. *Pet. Explor. Dev.* **2017**, *44*, 758−769.

(27) Lu, X.; Wang, Y.; Yang, D.; Wang, X. Characterization of paleo-karst reservoir and faulted karst reservoir in Tahe Oilfield, Tarim Basin China. *Adv. Geo-Energy Res.* **2020**, *4*, 339−348.

(28) He, B.; Xu, Y. G.; Wang, Y. M.; Xiao, L. Nature of Dongwu movement and its temporal and spatial evolution. *J. China Univ. Geosci.* **2005**, *30*, 89−96.

(29) Su, W.; Jiang, Q.; Chen, Z.; Wang, Z.; Jiang, H.; Bian, C.; Feng, Q.; Wu, Y. Sequence stratigraphic features of the Middle Permian Maokou Formation in the Sichuan Basin and their controls on source rocks and reservoirs. *Nat. Gas Ind. B* **2015**, *2*, 421−429.

(30) Jiang, Q.; Hu, S.; Jiang, H.; Zhai, X.; Ren, M.; Chen, X.; Li, Q.; Zhang, Y. Calculation and inducement of lacuna in the Mid-Permian Maokou Fm of Sichuan Basin. *Nat. Gas Ind. B* **2018**, *5*, 351−359.

(31) Wang, X.; Zhang, X.; Gao, F.; Zhang, M. Astronomical Cycles of the Late Permian Lopingian in South China and Their Implications for Third-Order Sea-Level Change. *J. Ocean Univ. China* **2020**, *19*, 1331−1344.

(32) Hays, J. D.; Imbrie, J.; Shackleton, N. J. Variations in the Earth's orbit: pacemaker of the ice ages. *Science* **1976**, *194*, 1121−1132.

(33) Yang, R. C.; Tian, Y. Discussion on the scientific issues in frontiers of astronomical cycles and hyperpycnal flow deposits. *Unconv. Oil Gas* **2020**, *7*, 1−8.

(34) Berger, A.; Loutre, M. F.; Laskar, J. Stability of the astronomical frequencies over the Earth's history for paleoclimate studies. *Science* **1992**, *255*, 560−566.

(35) Shi, J.; Jin, Z.; Liu, Q.; Zhang, R.; Huang, Z. Cyclostratigraphy and astronomical tuning of the middle ocene terrestrial successions in the Bohai Bay Basin Eastern China. *Global Planet Change* **2019**, *174*, 115−126.

(36) Cong, F.; Zhu, F.; Cai, Z.; Chen, H.; Li, J.; Wang, Y.; Wang, L. Orbitally forced glacio-eustatic origin of third-order sequences and parasequences in the Middle Permian Maokou Formation, South China. *Mar. Pet. Geol.* **2019**, *99*, 237−251.

(37) Fang, Q.; Wu, H.; Hinnov, L. A.; Jing, X.; Wang, X.; Yang, T.; Li, H.; Zhang, S. Astronomical cycles of Middle Permian Maokou Formation in South China and their implications for sequence stratigraphy and paleoclimate. *Palaeogeogr., Palaeoclimatol., Palaeoecol.* **2017**, *474*, 130−139.

(38) Xiao, Z.; Ding, W.; Hao, S.; Taleghani, A. D.; Wang, X.; Zhou, X.; Sun, Y.; Liu, J.; Gu, Y. Quantitative analysis of tight sandstone reservoir heterogeneity based on rescaled range analysis and empirical mode decomposition: A case study of the Chang 7 reservoir in the Dingbian oilfield. *J. Pet. Sci. Eng.* **2019**, *182*, 106326−106311.

(39) Jia, D. L.; Tian, J. C.; Lin, X. B.; Yang, G. H.; Feng, W. X.; Zhang, X.; Tang, Y.; Yang, C. Y. Milankovitch cycles in the Silurian Kepingtage Formation in Shuntuoguole area, Tarim Basin. *Oil Gas Geol.* **2018**, *39*, 749−758.

(40) Feng, B.; Li, H.; He, Y. B.; Su, S. Y. Characteristics of Milankovitch cycles in deep water contourites: a case study of Upper Ordovician Zhaolaoyu Formation in Fuping area of Shanxi, China. *J. Earth Sci. Environ.* **2019**, *41*, 69−82.

(41) Gao, F.; Wang, N. X.; Qiao, X. Y.; Liu, P. Dolomite diagenetic environments analysis based on ancient salinity and ancient water temperature: A case study of M51 sub-members of Majiagou Formation in Yanchang Area of Southeast Ordos Basin. *Unconv. Oil Gas* **2019**, *6*, 47−53.

(42) Zhang, X.; Pang, X.; Jin, Z.; Hu, T.; Toyin, A.; Wang, K. Depositional model for mixed carbonate-clastic sediments in the

Middle Cambrian Lower Zhangxia Formation, Xiaweidian, North China. *Adv. Geo-Energy Res.* **2020**, *4*, 29−42.

(43) Liu, G. C.; Jin, Z. J.; Li, J. C. A new method on the quantitative study of depositional and erosional processes of sedimentary basins: an application of wave process analysis during basin evolution. *ACTA Sediment. Sin.* **1995**, *13*, 23−31.